Geophysical Journal International

Geophys. J. Int. (2012) **189,** 1223–1236 doi: 10.1111/j.1365-246X.2012.05390.x

Fault kinematics in northern Central America and coupling along the subduction interface of the Cocos Plate, from GPS data in Chiapas (Mexico), Guatemala and El Salvador

A. Franco,[1]* C. Lasserre,[2] H. Lyon-Caen,[1] V. Kostoglodov,[3] E. Molina,[4,]† M. Guzman-Speziale,[5] D. Monterosso,[6] V. Robles,[7] C. Figueroa,[8] W. Amaya,[8] E. Barrier,[9] L. Chiquin,[10] S. Moran,[10] O. Flores,[11] J. Romero,[12] J. A. Santiago,[3] M. Manea[3] and V. C. Manea[3]

[1]*Laboratoire de Géologie, Ecole Normale Supérieure, CNRS, Paris, France. E-mail: franco@geologie.ens.fr*
[2]*ISTerre, Université de Grenoble 1, CNRS, F-*38041 *Grenoble, France*
[3]*Instituto de Geofísica, Universidad Nacional Autónoma de México, Mexico*
[4]*Instituto Nacional de Sismología, Vulcanología, Meterología e Hidrologia,Guatemala Ciudad, Guatemala*
[5]*Centro de Geosciencias, UNAM, Campus Juriquilla, Mexico*
[6]*Coordinadora Nacional para la Reduccion de Desastres, Guatemala Ciudad, Guatemala*
[7]*Instituto Geografico Nacional, Guatemala Ciudad, Guatemala*
[8]*Instituto Geográfico y Catastro Nacional, Centro Nacional de Registros, El Salvador*
[9]*Institut des sciences de la Terre de Paris, CNRS, Université Pierre et Marie Curie, Paris, France*
[10]*Centro Universitario del Norte, Universidad de San Carlos de Guatemala, Coban, Guatemala*
[11]*Centro de Estudios Superiores de Energia y Minas, Universidad de San Carlos de Guatemala, Guatemala Ciudad, Guatemala*
[12]*Geologia Ambiental e Economia, Guatemala Ciudad, Guatemala*

Accepted 2012 January 20. Received 2012 January 11; in original form 2011 August 8

SUMMARY

New GPS measurements in Chiapas (Mexico), Guatemala and El Salvador are used to constrain the fault kinematics in the North America (NA), Caribbean (CA) and Cocos (CO) plates triple junction area. The regional GPS velocity field is first analysed in terms of strain partitioning across the major volcano-tectonic structures, using elastic half-space modelling, then inverted through a block model. We show the dominant role of the Motagua Fault with respect to the Polochic Fault in the accommodation of the present-day deformation associated with the NA and CA relative motion. The NA/CA motion decreases from 18–22 mm yr^{-1} in eastern Guatemala to 14–20 mm yr^{-1} in central Guatemala (assuming a uniform locking depth of 14–28 km), down to a few millimetres per year in western Guatemala. As a consequence, the western tip of the CA Plate deforms internally, with $\simeq$9 mm yr^{-1} of east–west extension ($\simeq$5 mm yr^{-1} across the Guatemala city graben alone). Up to 15 mm yr^{-1} of dextral motion can be accommodated across the volcanic arc in El Salvador and southeastern Guatemala. The arc seems to mark the northern boundary of an independent forearc sliver (AR), pinned to the NA plate. The inversion of the velocity field shows that a four-block (NA, CA, CO and AR) model, that combines relative block rotations with elastic deformation at the block boundaries, can account for most of the GPS observations and constrain the overall kinematics of the active structures. This regional modelling also evidences lateral variations of coupling at the CO subduction interface, with a fairly high-coupling ($\simeq$0.6) offshore Chiapas and low-coupling ($\simeq$0.25) offshore Guatemala and El Salvador.

Key words: Satellite geodesy; Seismic cycle, Plate motions, Subduction zone processes; Dynamics and mechanics of faulting; Kinematics of crustal and mantle deformation.

1 INTRODUCTION

The complex surface deformation observed in northern Central America results from the interaction between the North America (NA), Cocos (CO) and Caribbean (CA) plates (Fig. 1). The main

*Now at: Laboratoire de Géodynamique des rifts et des Marges passives, Université du Maine, UMR6115, Le Mans, France.
†Now at: Universidad Mariano Gálvez, Guatemala Ciudad, Guatemala.

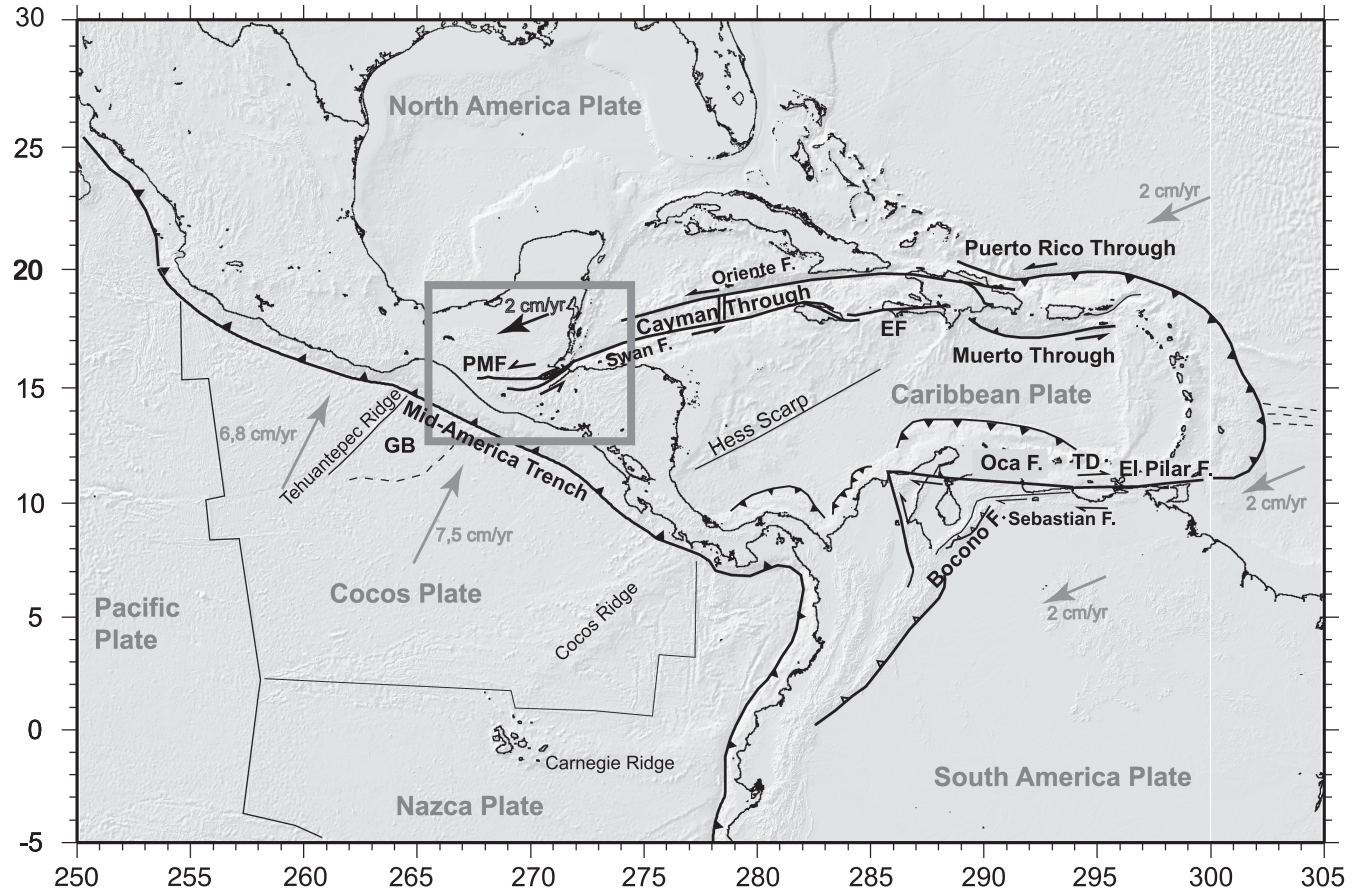

Figure 1. Tectonic setting of the Caribbean Plate. Grey rectangle shows study area of Fig. 2. Faults are mostly from Feuillet *et al.* (2002). PMF, Polochic–Motagua faults; EF, Enriquillo Fault; TD, Trinidad Fault; GB, Guatemala Basin. Topography and bathymetry are from Shuttle Radar Topography Mission (Farr & Kobrick 2000) and Smith & Sandwell (1997), respectively. Plate velocities relative to Caribbean Plate are from Nuvel1 (DeMets *et al.* 1990) for Cocos Plate, DeMets *et al.* (2000) for North America Plate and Weber *et al.* (2001) for South America Plate.

active structures related to this interaction are the Polochic and Motagua left-lateral strike-slip faults at the NA/CA boundary, the north-striking grabens south and east of it in Guatemala and Honduras, the Mid-America Trench (MAT) and the volcanic arc associated with the CO subduction under the CA Plate (e.g. Plafker 1976; Burkart 1983; Burkart & Self 1985). In the past decade, several seismological and geodetic studies have tried to quantify the kinematics of these structures accommodating the active deformation (e.g. DeMets 2001; Guzman-Speziale 2001; Lyon-Caen *et al.* 2006) and to understand the different factors and the tectonic forces that control this deformation (e.g. Alvarez-Gomez *et al.* 2008; Correa-Mora *et al.* 2009; Rodriguez *et al.* 2009).

From GPS measurements and modelling, Lyon-Caen *et al.* (2006) documented a 20 mm yr^{-1} rate of the NA/CA relative motion in easternmost Guatemala, mostly accommodated across the Motagua Fault (MF). This rate decreases westwards, reaching nearly 0 mm yr^{-1} near the Mexico-Guatemala border, as part of the deformation is being transferred southwards into the grabens (mainly the Guatemala city graben). Lyon-Caen *et al.* (2006) also suggest a weak coupling at the CO/CA subduction interface and a dextral slip component across the volcanic arc in Guatemala. More recent studies (Correa-Mora *et al.* 2009; Rodriguez *et al.* 2009; Alvarado *et al.* 2011) have used a dense GPS network in Honduras, El Salvador and Nicaragua to build a regional model of the deformation of the western part of the CA Plate. A main outcome is that the extension relative to the stable CA plate is not limited to Guatemala but is observed in a broader area (Guatemala and western Honduras, Rodriguez *et al.* 2009). Another important result is that coupling at the CO/CA subduction interface offshore El Salvador and Nicaragua, inferred from finite element modelling (Álvarez-Gómez *et al.* 2008; Correa-Mora *et al.* 2009), is likely weak as well. These models also suggest that the volcanic arc is a rheologically weak zone. It separates the undeformed, trench-parallel moving forearc, which is pinned to the NA Plate (Correa-Mora *et al.* 2009; Alvarado *et al.* 2011), and the wedge-shaped western CA Plate, whose inner deformation is influenced by the direction of the NA/CA motion relatively to the strike of the curved Polochic–Motagua fault (PMF) system (Álvarez-Gómez *et al.* 2008; Rodriguez *et al.* 2009).

In this paper, we densify the Lyon-Caen *et al.* (2006) data set including a third campaign of GPS measurements in Guatemala. We also extend the study area using new GPS measurements in Chiapas (southern Mexico) and El Salvador. This allows us not only to refine previous results but also to complement the regional data set and to propose a kinematic block model in the critical area of the triple junction between the CO/CA/NA plates. In particular, we discuss the present-day GPS-derived coupling along the subduction zone from southern Mexico to El Salvador.

We first present the GPS data set, the processing strategy and a first-order analysis of the GPS velocity field in terms of strain partitioning across the major volcano-tectonic structures. The GPS velocity field at the regional scale is then inverted using the DEFNODE model that combines relative block rotations and elastic

deformation due to coupling at the block boundaries (McCaffrey 2002). Finally, we discuss the implication of this new data set and modelling for the understanding of the complex regional tectonics.

2 DATA AND PROCESSING

2.1 GPS sites and data acquisition

We use GPS data from 34 campaign sites (Fig. 2, Table 1): 23 sites in Guatemala, three sites in El Salvador and eight sites in Chiapas (southern Mexico). Data from four regional permanent stations belonging to the Servicio Sismologia Nacional (SNN) mexican network (site TPCH) or to the International GPS Service (IGS) network (sites ELEN, HUEH, SSIA) complement this campaign data set (Fig. 2).

The first two campaigns of measurements in Guatemala were carried out in 1999 February and 2003 and are described in Lyon-Caen *et al.* (2006). Remeasurements were done in January 2006, (including six new sites first measured in 2003) using nine Ashtech ZXtrem receivers with Geodetic IV antennas, and three Trimble 5700 receivers with Zephyr Geodetic antennas. All sites were occupied for at least two sessions of 12–24 hr, with two sites that were measured continuously during 6 and 10 d (PIN and COB, respectively, Fig. 2), as in 1999 and 2003.

The three sites in El Salvador were measured in 2003 February during the campaign in Guatemala, with 48 hr of occupation at each site, using Ashtech Z12 receivers and Geodetic III and IIA antennas. They were remeasured in 2006 March using Z-Max Thales receivers and antennas, together with the ZAC Guatemalan site (Fig. 2), during four consecutive, 10-hr-long daily sessions.

Measurements in Chiapas, conducted by Universidad Nacional Autónoma de Mexico (UNAM), began in 2002 and were repeated each year until 2005. Leica SR520 receivers were used with Leica A504 Dorne Margelin antennas. Each site was measured during two to five 24-hr sessions. Table S1 in the Supporting Information summarizes the sites' occupation.

2.2 Processing strategy

We use the GAMIT software (King & Bock 2002) to process data from the campaign and permanent stations mentioned above. The GAMIT unconstrained solutions of daily station coordinates and their associated covariances are combined with selected Scripps Orbital and Permanent Array Center (SOPAC) solutions, using GLOBK (Herring 2002), to obtain stations positions and velocities in the ITRF2000 reference frame. Velocity uncertainties are estimated using a Markovian error model during the GLOBK daily solution combination (Herring 2002). We authorize for each station a random walk of 2 mm per$\sqrt{\text{yr}}$ around their position. Velocity vectors are determined without introducing a Markovian noise.

Several earthquakes occurred within our regional network between 1999 and 2006. We select all earthquakes with a hypocentral depth shallower than 30 km, and the $M_{\text{w}} \geq 6$ deeper earthquakes that are located within 500 km from the centre of our study area (15.1°N, 269.7°E). We estimate their rupture parameters (slip and rupture size), based on the CMT catalogue and scaling laws (Wells & Coppersmith 1994). For 2001, $M_{\text{w}} = 7.7$ earthquake in El Salvador in particular, these parameters are given by Bommer *et al.* (2002) and Vallée *et al.* (2003). We use an elastic half-space model (Okada 1985) to estimate the cumulative coseismic displacements associated with the selected earthquakes at each GPS site (Tables S2 and S3), and take them into account during the GLOBK combination process. This changes velocities by up to 1.8 mm yr^{-1}

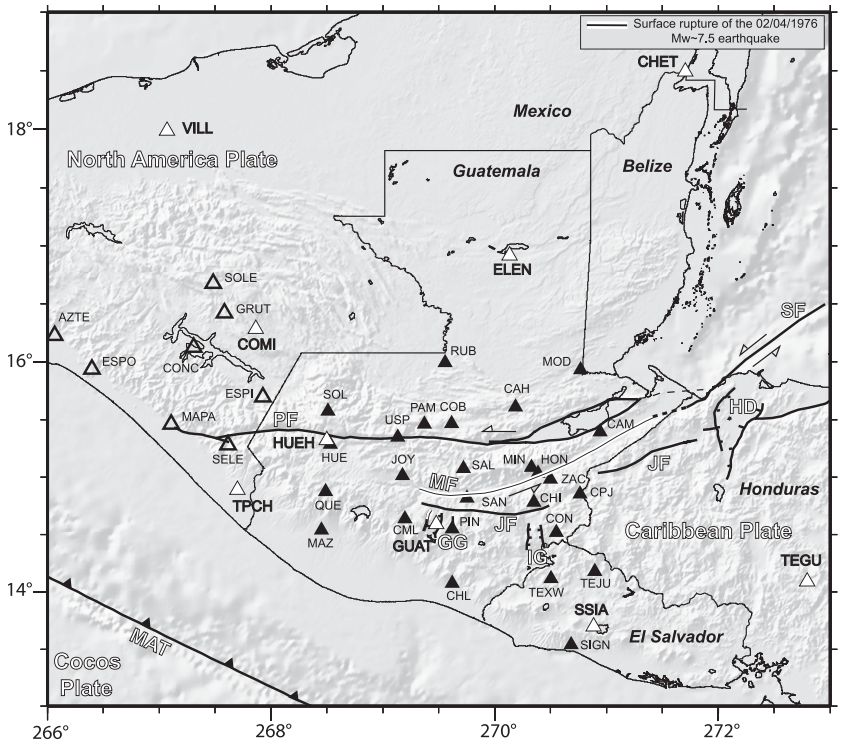

Figure 2. GPS network: campaign sites in Guatemala/El Salvador (black triangles), Chiapas and Mexico (open triangles) and permanent sites (white triangles with names in bold). MAT, Mid-America Trench; PF, Polochic Fault; MF, Motagua Fault; JF, Jocotan Fault; GG, Guatemala city Graben; IG, Ipala Graben; HD, Honduras Depression; SF, Swan Fault.

Table 1. GPS sites information. Lon, Lat, $V_e, V_n, \sigma_e, \sigma_n, \sigma$ are longitude, latitude, east and north velocities referenced to ITRF2000, east and north standard errors and form factor, respectively. Sites in bold are permanent sites.

Lon (°E)	Lat (°N)	V_e	V_n	σ_e	σ_n	σ	Site
			Chiapas				
266.063	16.225	−5.46	1.53	1.27	1.23	−0.027	AZTE
267.307	16.125	−2.61	5.67	1.30	1.23	−0.017	CONC
267.927	15.696	−1.25	6.86	1.28	1.23	−0.021	ESPI
266.396	15.935	−4.98	4.63	1.27	1.23	−0.024	ESPO
267.143	16.419	−4.84	1.71	1.56	1.50	0.002	GRUT
267.106	15.459	−2.00	4.33	1.27	1.23	−0.023	MAPA
267.611	15.281	−2.07	9.92	1.28	1.23	−0.041	SELE
267.481	16.675	−4.64	4.12	1.30	1.23	−0.014	SOLE
267.704	14.883	−0.96	6.72	1.53	1.49	−0.026	**TPCH**
			Guatemala				
270.182	15.605	−3.25	0.44	1.29	1.16	0.028	CAH
270.941	15.394	−0.3	−0.66	1.38	1.21	0.075	CAM
270.348	14.779	9.25	4.71	1.25	1.14	0.053	CHI
269.618	14.075	5.45	4.79	1.36	1.18	0.026	CHL
269.196	14.638	2.33	0.87	1.25	1.14	0.035	CML
269.611	15.464	−2.53	0.24	1.20	1.10	0.087	COB
270.548	14.517	12.73	4.84	1.26	1.15	0.040	CON
270.760	14.854	5.09	3.22	1.87	1.23	0.052	CPJ
270.132	16.916	−6.78	−0.32	1.21	1.19	0.024	**ELEN**
269.478	14.590	3.20	2.80	1.71	2.40	−0.118	**GUAT**[a]
270.385	15.030	1.89	0.74	1.31	1.19	0.026	HON
268.531	15.282	−1.24	1.03	1.31	1.17	0.052	HUE
268.497	15.318	−2.65	3.76	1.22	1.20	0.063	**HUEH**
269.174	15.011	−3.22	0.36	1.27	1.21	0.003	JOY
268.450	14.537	2.55	3.16	1.66	1.47	−0.200	MAZ
270.329	15.084	1.42	1.41	1.26	1.15	0.039	MIN
270.766	15.930	−5.63	0.36	1.31	1.21	0.040	MOD
269.370	15.458	−2.42	4.7	1.23	1.20	0.043	PAM
269.620	14.551	7.62	2.39	1.20	1.10	0.098	PIN
268.486	14.871	0.53	−2.51	1.28	1.14	0.051	QUE
269.553	15.990	−5.52	0.73	1.26	1.15	0.046	RUB
269.719	15.075	0.09	1.38	1.29	1.16	0.038	SAL
269.751	14.816	6.02	1.41	1.26	1.15	0.054	SAN
268.506	15.571	−2.61	1.37	1.29	1.16	0.044	SOL
269.130	15.348	−5.08	−1.92	1.24	1.20	0.061	USP
270.499	14.981	5.45	4.92	1.47	1.30	0.012	ZAC
			El Salvador				
270.680	13.495	−0.69	13.05	1.39	1.29	0.010	SIGN
270.883	13.697	4.48	8.60	1.40	1.00	0.500	**SSIA**
270.895	14.175	10.37	5.39	1.38	1.29	0.010	TEJU
270.500	14.116	12.67	5.17	1.38	1.29	0.010	TEXW
			Honduras				
272.794	14.090	8.90	5.70	1.60	1.20	0.000	**TEGU**[a]

[a]Indicates velocities calculated by DeMets *et al.* (2007).

for site CON in eastern Guatemala (Fig. 2) but no more than 1 mm yr^{-1} for the other sites.

Due to the short overlapping in time between measurements made within the Guatemala/El Salvador subnetwork, and those made within the Chiapas subnetwork (Table S1), we first compute two independent GLOBK velocity solutions for these two subnetworks, following the procedure described earlier. Whereas both referenced to ITRF2000 with comparable residuals (∼5 mm on positions, 1.3 mm yr^{-1} on velocities for Guatemala/El Salvador and ∼4.5 mm on positions, 2.5 mm yr^{-1} on velocities for Chiapas), the two resulting velocity fields are not fully consistent, with common sites such as TPCH showing different velocity vectors (Fig. S1a). To make both velocity fields consistent, we use the more robust Guatemala/El Salvador solution as a reference, and we estimate the angular velocity that best adjusts the Chiapas velocity vectors with the Guatemala/El Salvador ones, at the common regional site TPCH and at the IGS stations used by GLOBK for the stabilization in ITRF2000 (Fig. S1a). We use the same strategy to adjust the resulting Guatemala–El Salvador–Chiapas velocity field to that of DeMets *et al.* (2007) in ITRF2000 (Fig. S1b). Angular velocities used to obtain the ITRF2000 velocities (Table 1) are listed in Table S4.

This procedure allows us to use the CA/ITRF2000 and NA/ITRF2000 angular velocities estimated by DeMets *et al.* (2007; Table S5) to reference our final regional velocity field in the CA and NA reference frames (Fig. 3). Note that we do not propagate the

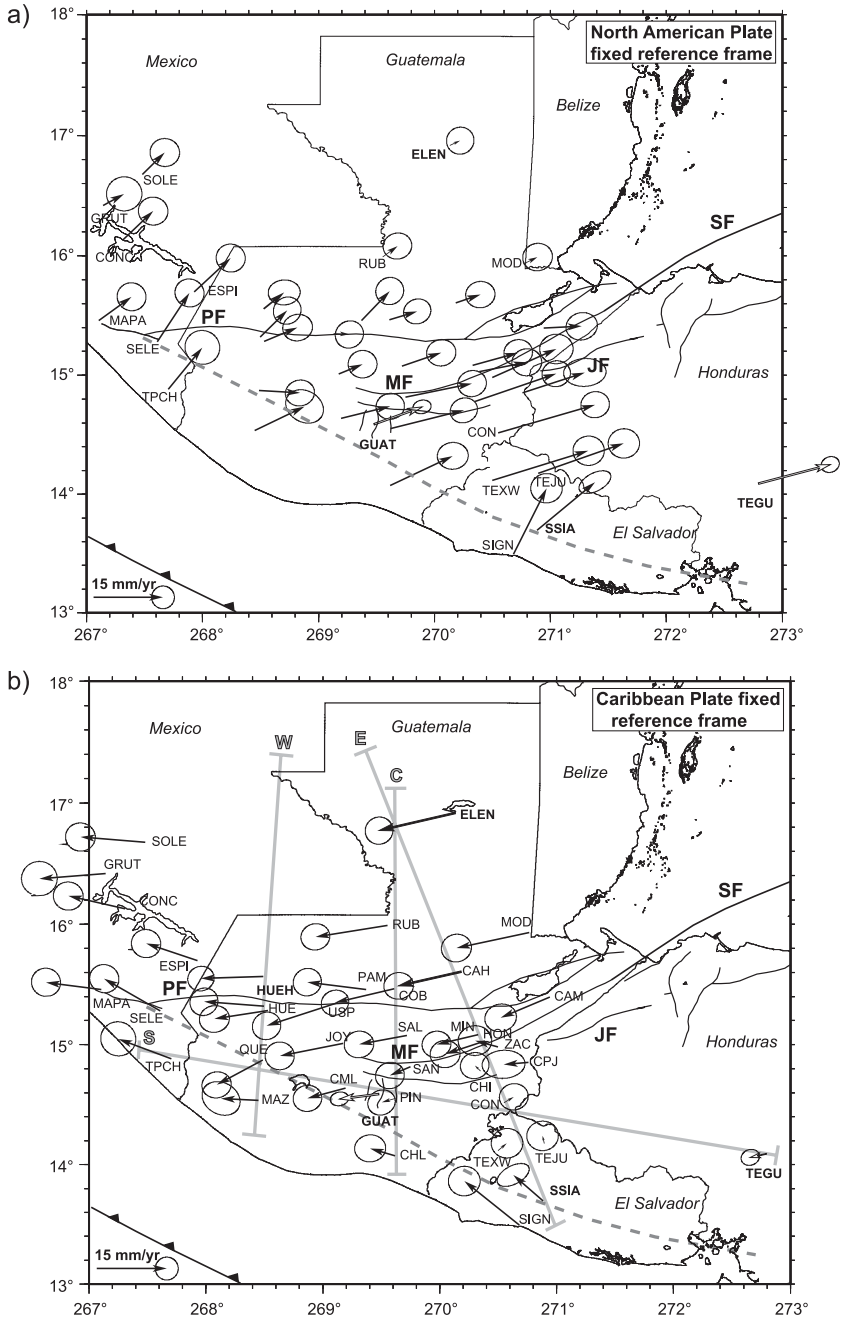

Figure 3. GPS velocity field from Table 1 in (a) North America and (b) Caribbean plates reference frames. Euler NA/ITRF2000 and CA/ITRF2000 angular velocities as well as velocity vectors of sites GUAT and TEGU (white arrows) are from DeMets *et al.* (2007). Dark grey bold lines outline active faults (names as in Fig. 2). Light grey lines indicate location of profiles shown in Fig. 4. Dotted line follows volcanic arc.

uncertainties of the angular velocities into the uncertainties of our sites velocities in these two frames. We estimate them to be on the order of 1 mm yr^{-1} at our regional stations, by comparison with velocity fields obtained using different values of the CA/ITRF2000 and NA/ITRF2000 angular velocity within their error bars. We neglect them in the following.

3 GPS VELOCITY FIELD AND ANALYSIS AT FAULT SCALE

Fig. 3 illustrates the complexity of the velocity field in the CO/CA/NA triple junction area. We first describe its main features in the NA and CA reference frames before analysing the slip partitioning among the different faults, the volcanic arc and the subduction zone.

3.1 Overall description

In the NA reference frame, the three sites ELEN, RUB and MOD, to the north, form a consistent group with small residual velocities (Fig. 3a), comparable to those of sites CHET, VILL and CAMP on the Yucatan Peninsula. On the first order, they can be considered as part of the stable NA Plate, as the Yucatan sites (Márquez-Azúa & DeMets 2009).

In the CA reference frame, the three sites CON, TEXW and TEJU show small residual velocities and can be considered at the

first order as representing the stable CA Plate (Fig. 3b). In the western, wedge-shaped part of the plate in between the MF and the volcanic arc, an east–west internal extension is observed across the grabens, confirming results from Lyon-Caen *et al.* (2006).

Fig. 3 also shows the overall left-lateral motion between the NA and CA plates and the associated velocity gradient across the PMF. In the NA frame, all stations in Chiapas have a consistent motion towards north-east, roughly perpendicular to the trench, suggesting coupling at the CO/NA slab interface (Fig. 3a). In contrast, in the CA frame, the velocities of the coastal sites south of the volcanic arc are mostly trench-parallel (Fig. 3b). This could result from a low coupling at the CO/CA slab interface, as already proposed by Lyon-Caen *et al.* (2006). However, the velocities in El Salvador also indicate a right-lateral motion across the volcanic arc relatively to the stable CA plate (Fig. 3b). The velocity field in southern Guatemala thus reflects the combined effects of coupling at the CO/CA interface and motion across the arc.

3.2 Strain partitioning across the major tectonic structures

Assuming first that the effect of the CO subduction on the velocity field is low in Guatemala and El Salvador (Lyon-Caen *et al.* 2006), we quantify the slip rates across the PMF, the grabens south of them and the volcanic arc, and refine the previous analysis by Lyon-Caen *et al.* (2006), taking advantage of the network densification and remeasurement. We project the ITRF2000 velocities along three north–south trending profiles (East E, Central C and West W) roughly perpendicular to the PMF (Figs 3b, 4a, 4d and 4f). We also project the horizontal CA-fixed velocities along a southern, east–west trending profile (South S) perpendicular to the grabens (Figs 3b and 5).

3.2.1 The PMF zone

We first use a one fault, half-space elastic model (e.g. Savage & Burford 1973) as in Lyon-Caen *et al.* (2006). We invert for the interseismic velocity, the locking depth and the location of the fault trace along profiles E and C (Figs 4a–e). Although strain accumulation is clearly concentrated on the northern trace of the MF on profile E, it seems offset by ∼15 km north of it on profile C. Based on the $\chi^2 = 1$ contour, the far-field velocity and locking depth ranges are 18–22 mm yr^{-1} (best-fit 20 mm yr^{-1}) and 14–28 km (best-fit 20 km) for profile E (best-constrained model) and 14–26 mm yr^{-1} (best-fit 20 mm yr^{-1}) and 12–66 km (best-fit 39 km) for profile C. The 20 km best-fit locking depth for profile E is consistent with the maximum depth of the seismogenic zone across the PMF system, derived from the present crustal seismicity distribution (Franco *et al.* 2009). We thus assume a constant 20-km locking depth along the entire fault system, and favour a model with a velocity of 20 mm yr^{-1} across profile E, decreasing to 16 mm yr^{-1} across profile C (Figs 4a–e). At least 4 mm yr^{-1} seems to be accommodated by the PMF across profile W (velocity difference between SOL and QUE, Fig. 4f), although the limited length of the profile and its small number of sites do not allow any elastic modelling.

The new data set and analysis thus confirm the decrease of the far-field velocity across the PMF from eastern to western Guatemala, probably tending towards zero in the triple junction area. It also confirms the dominant role of the MF with respect to the Polochic Fault in the accommodation of the deformation associated with the NA and CA relative motion (Lyon-Caen *et al.* 2006). An homogeneous half-space elastic model including the two faults (with a fixed location) shows that at least 88 per cent of the total strain is accommodated by the MF in the eastern part of Guatemala (Fig. 4c). This fault is generally considered as the geological boundary between the NA and the CA plates (e.g. Carfantan 1986; Donelly *et al.* 1990; Martens *et al.* 2007). However, the area in between the Polochic and Motagua faults is a wide complex metamorphic zone. Furthermore, there is no doubt on the Holocene activity of the Polochic Fault as attested by the similarities of its morphology, Holocene slip rate, historical and present-day seismicity with that of the MF (Carr 1976; Burkart 1978; Schwartz *et al.* 1979; Burkart 1983; White 1985; White & Harlow 1993; Ambraseys & Adams 2001; Kovach 2004; Franco *et al.* 2009; Suski *et al.* 2009). The lack of strain accumulation across the Polochic Fault remains a puzzling result. We investigate below the possible influence of rigidity contrasts across the PMF zone and of post-seismic effects following the 1976 earthquake on the present-day velocity field.

A recent Receiver Function study suggests variations of the Moho depth (resp. V_p/V_s ratio) across the PMF (Franco *et al.* 2009), with a Moho depth thinner by 4–6 km (resp. a V_p/V_s decreased by 6–7 per cent) in between the two faults. Such variations, that are likely related to the geological history of this region, could result in asymmetric velocity profiles across faults, associated with contrasts in elastic parameters or elastic thicknesses on both sides of the faults (Le Pichon *et al.* 2005; Schmalzle *et al.* 2006; Chéry 2007; Jolivet *et al.* 2008). Our tests on velocities of profile E, using a modified half-space elastic model taking into account asymmetry (formulation of Le Pichon *et al.* 2005), still show that the Polochic Fault does not accommodate more than ∼15 per cent of the total deformation (Fig. 4c).

To estimate the contribution to the present-day velocity field of post-seismic relaxation related to the 1976 earthquake, we use a 3-D viscoelastic model developed by Yu *et al.* (1996). We consider an elastic layer, with a thickness H = 30 km and a shear modulus $\mu = 3 \times 10^{10}$ N m, above an homogeneous viscous half-space, characterized by a viscosity η ranging from 10^{18} to 10^{21} Pa s. The 1976 rupture on the MF is modelled using an infinitely long vertical fault extending from the surface to a depth of 15 km, with an homogeneous coseismic slip of 1.5 m consistent with field observations by Plafker (1976). Fig. S2 shows the modelled post-seismic displacements as a function of time normalized by the relaxation time ($\frac{t}{\tau}$, with $\tau = 2\frac{\eta}{\mu}$), for various distances y from the fault. Maximum velocities related to post-seismic relaxation are on the order of 0.6 mm yr^{-1}: 0.4 cm between the 1999 and 2006 GPS campaigns, at a distance of 40 km from the MF trace and for a viscosity of 10^{19} Pa s. In any case, we conclude that post-seismic effects cannot explain the apparent lack of strain accumulation across the Polochic Fault.

3.2.2 East–West extension

The southern profile S shows an extension rate of ∼9 mm yr^{-1} across the CA graben series north of the volcanic arc, between sites TEJU to the east and TPCH in southwestern Chiapas (Fig. 5). This gives only a first-order estimate as we do not take into account the rotation of microblocks separating the active grabens. Most of the extension is concentrated across the Guatemala city grabens (rate of 5 ± 2 mm yr^{-1}), which confirms previous estimation by Lyon-Caen *et al.* (2006). The remaining extension, given our GPS network geometry and error bars, is not clearly localized on specific structures. Seismicity and fault plane solutions (Guzman-Speziale 2001; Caceres *et al.* 2005; Franco *et al.* 2009), as well as complementary GPS observations (Rodriguez *et al.* 2009; note that data are referenced to ITRF2005 instead of ITRF2000 in this study) and finite element modelling (Alvarez-Gomez *et al.* 2008) in northern Central

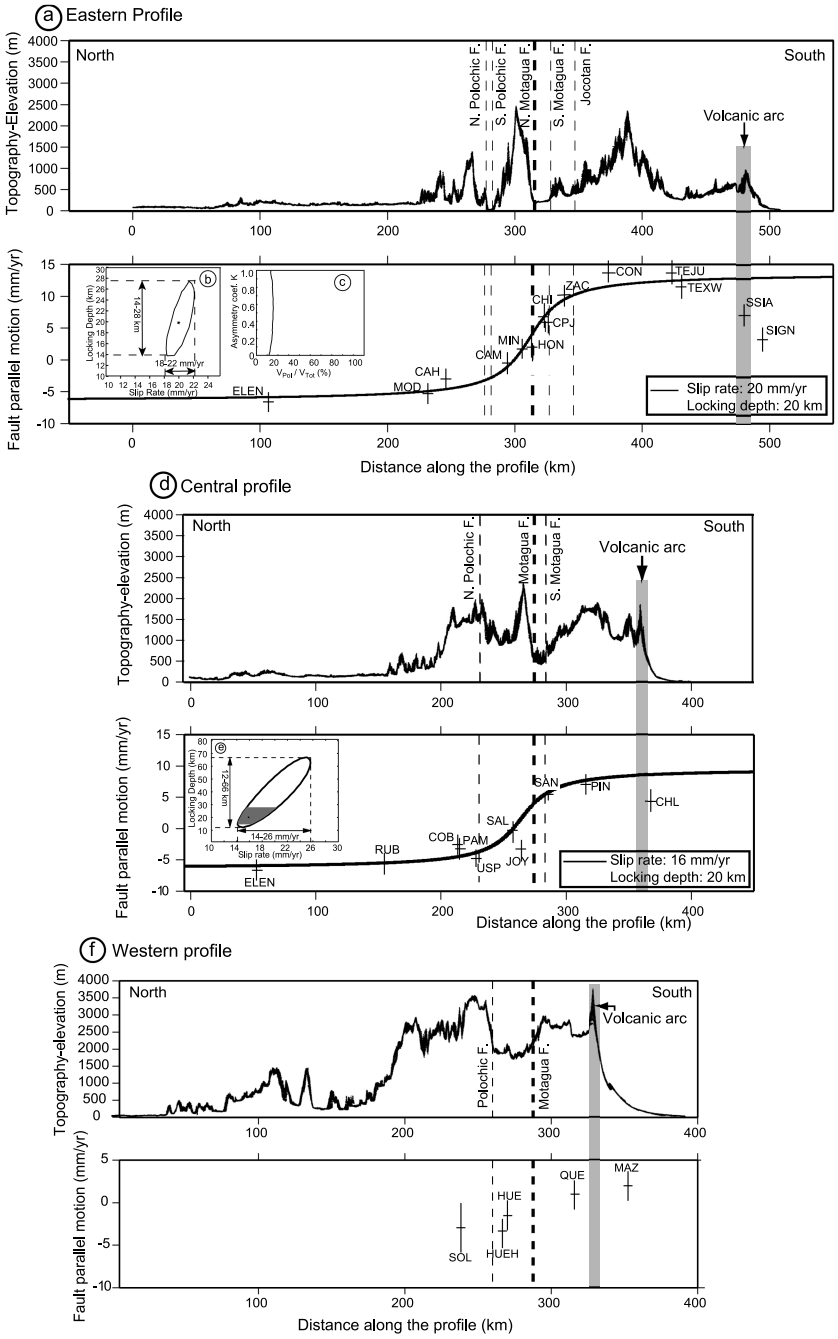

Figure 4. (a) Topography (top panel) and ITRF2000 GPS velocities projected onto fault-parallel components along eastern profile, E (bottom), with fit model for a locking depth of 20 km. Main active fault traces are indicated by dotted lines. Volcanic arc area is shaded. (b) $\chi^2 = 1$ contour line for locking depth and rate estimated using half-space elastic modelling (see Section 3 in text). Cross shows model for a 20-km locking depth (best-fit). (c) $\chi^2 = 1$ contour line for a two-fault model, showing the relative contribution of the Polochic Fault to the NA/CA motion, as a function of the asymmetry coefficient K across fault (Le Pichon *et al.* 2005). Case $K = 0$ corresponds to an homogeneous half-space model. (d) and (e) Same as (a) and (b), respectively, for central profile, C. Shaded area on (e) is that consistent with the locking depth range estimated from eastern profile in (b). (f) same as (a) and (d) for western profile, W. See Fig. 3 for the location of profiles.

America indicate that some extension is accommodated eastward from Guatemala city, up to northeastern Honduras, across the Ipala Graben and the depression of Honduras in particular.

3.2.3 Volcanic arc

In the CA Plate reference (Fig. 3b), GPS sites along the coast in Guatemala and El Salvador (TPCH, MAZ, CHL, SIGN, SSIA) show velocity vectors parallel to the MAT, consistent with dextral motion across the volcanic arc at a rate of up to 14 mm yr^{-1} in El Salvador (see TEJU–SSIA–SIGN velocity gradient in Fig. 4a). Such dextral shear is in agreement with previous GPS measurements in Guatemala by Lyon-Caen *et al.* (2006). Similar rates are also observed by GPS in El Salvador and Nicaragua ($\simeq$15 mm yr^{-1}, Turner *et al.* 2007; Correa-Mora *et al.* 2009; Alvarado *et al.* 2011) and Costa-Rica (Norabuena *et al.* 2004) or attested by dextral

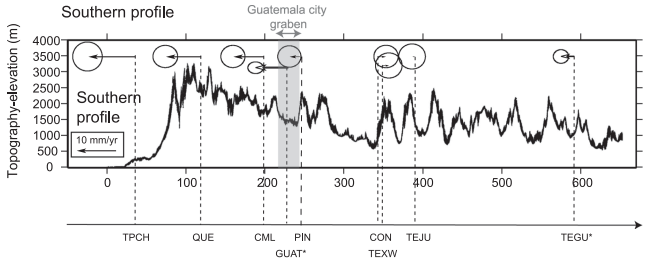

Figure 5. Topography and GPS vectors in CA Plate reference frame projected perpendicularly to the mean grabens orientation along southern profile, S. Sites names are indicated at bottom. See Fig. 3 for the location of profiles.

Table 2. Selected earthquakes from CMT-Harvard catalogue with slip vector azimuths to constrain slip direction along the subduction (see Section 4 in text).

Long. (°E)	Lat. (°N)	Azimuth (°)	Depth (km)	Magnitude CMT M_w	Reference CMT
272.84	12.7700	38	40.3	6.5	053178A
268.95	13.8800	33	25.0	6.3	103078A
270.36	13.1500	31	29.4	6.1	120678B
269.12	13.8300	27	29,8	6.8	102779A
269.27	13.7800	26	27.6	6.8	102779B
267.89	14.2700	36	42.6	5.9	040682A
268.06	14.0500	27	31.0	7.0	120283A
273.44	11.5900	34	54.6	6.1	082384A
273.44	11.9300	40	50.0	6.1	041985A

mechanisms of recent crustal earthquakes (M6.6, 2001 February 13 earthquake in El Salvador in particular, Canora *et al.* 2010). It can be interpreted as dextral slip on a northwest-striking, intraarc, subvertical fault, bounding to the north an independent forearc sliver. Such dextral fault system within the volcanic arc has been evidenced in the field in El Salvador (Martínez-Díaz *et al.* 2004; Corti *et al.* 2005). Satellite images and topography analysis suggest that it may continue westwards under the volcanic deposits in Guatemala (Carr 1976). In Nicaragua, Lafemina *et al.* (2002) suggest that the dextral shear is rather accommodated by bookshelf faulting involving northeast-striking left-lateral faults perpendicular to the trench. Slip partitioning related to the obliquity of the convergence of the CO Plate has been proposed to explain the observed dextral shear across the arc (DeMets 2001). However, it would require strong coupling along the subduction interface, in contradiction with the most recent studies (Lyon-Caen *et al.* 2006; Turner *et al.* 2007; Correa-Mora *et al.* 2009; this paper). Instead, the trench-parallel, northwestward, forearc motion may be related to the indentation of the CO Ridge on the CA Plate, offshore Costa Rica (LaFemina *et al.* 2009; Alvarado *et al.* 2011).

4 REGIONAL MODELLING OF THE VELOCITY FIELD

To refine the proposed first-order interpretation of the crustal deformation, we model the GPS velocity field using the 3D-inversion method DEFNODE developed by McCaffrey (2002). GPS velocities are considered as resulting from the combination of relative block rotations and elastic deformation due to coupling at the block boundaries. The relative block motions are defined by spherical Earth angular velocity vectors (Euler rotation poles and rates) while the interseismic deformation is modelled as backslip on the faults that separate blocks (Okada 1985; Savage 1983). The faults at the boundary of the finite blocks are defined in 3-D, by a series of nodes along the fault planes (forming an irregular grid of points along strike and downdip). Fault locking is parametrized at each node by a coupling factor ϕ, which represents the fractional part of the relative block motion that is not accommodated by steady, aseismic slip. ϕ ranges between 0 (no coupling) and 1 (full coupling). Block angular velocities and coupling factors ϕ can be inverted by minimizing the misfit between observations (e.g. GPS velocities and slip vectors) and predicted data, using a simulated annealing method.

4.1 Input data, model geometry

We constrain our models using the horizontal GPS velocities and their associated uncertainties listed in Table 1. However, given the poor density of points that defines the east–west extension in the westernmost part of the CA Plate, we cannot model this extension and do not take into account velocities at sites QUE, CML, GUAT and PIN (Fig. 3). We also use slip vectors of subduction earthquakes of $M_w \geq 5.9$ (Table 2) from the complete CMT catalogue, to provide constraints on the slip direction along the subduction plane.

We define two sets of model geometries: (1) a three-block (NA, CA and CO) and two-fault (MF and MAT) model, called 3B model hereafter, and (2) a four-block (NA, CA, CO, and the forearc microplate, AR) and three-fault model (MF, MAT and the Volcanic Arc Fault, VAF), called the 4B model (Fig. 6). The MF that marks the NA/CA boundary follows the MF surface trace to the east. To the west, we extrapolate this fault trace under the volcanic deposits, and connect it to the Polochic Fault near the Mexican border, then to the MAT (Figs 2 and 6). The MF is considered as a vertical fault. The VAF, defined as a vertical fault as well, is the continuation to the west, below the volcanic arc, of the well-known trace of the dextral fault that runs from Costa-Rica to northern Salvador (e.g. Corti *et al.* 2005). We use the bathymetry and the microseismicity distribution relocated by Engdhal & Villasenor (2002) to delineate the depth contours of the CO Plate slab (Fig. 6).

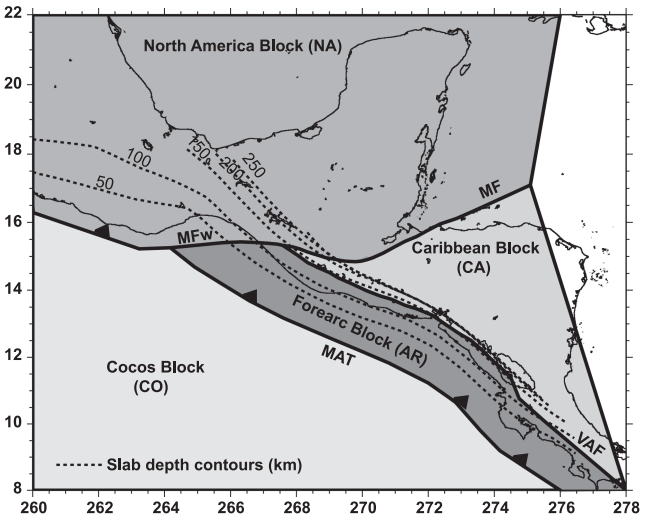

Figure 6. The four-block (4B) model geometry. The NA, CA, CO and AR blocks are delimited by three faults: the Mid-America Trench (MAT), the Volcanic Arc Fault (VAF) and the Motagua Fault (MF, noted MF_w west of its junction with VAF). The three-block (3B) model follows the same geometry, with AR and CA blocks combined into a single CA block.

4.2 Model parameters

For both the 3B and 4B models, the CO and NA angular velocity vectors relative to the CA block are from DeMets *et al.* (2007) and (1990) (Nuvel1-A), respectively. There is no clear evidence neither onland, nor offshore, nor in the seismic activity, that the western continuation of the MF west of its junction with the volcanic arc (named MF_w hereafter, Fig. 6), exists and is active. As we need to materialize all block limits between the CO/NA/CA plates in the DEFNODE model, we assign to MF_w a uniform full coupling, from the surface down to 250 km. This is equivalent in the model to considering that the AR block is pinned to the NA block (Alvarez-Gomez *et al.* 2008; Rodriguez *et al.* 2009). In any case, the geodetic data onland would not allow to test other hypothesis. We have tested that our main conclusions are not sensitive to this modelling choice.

In the 3B model, we invert for the coupling along the MF (east of MF_w, Fig. 6) and the MAT. In the 4B model, we fix the coupling along the MF according to the results from the 3B model and invert for the coupling along the VAF, MAT and for the AR/CA angular velocity (Fig. 6). We discuss the trade-off between the inverted parameters.

Along the MAT subduction interface, we assume that coupling can occur down to 25 km depth (Márquez-Azúa & DeMets 2003; Lyon-Caen *et al.* 2006). The locking depth along the MF is initially fixed to 20 km, as deduced from the analysis in Section 3.2.1, and to 15 km along the VAF (same order of magnitude as found eastward in El Salvador, Correa-Mora *et al.* 2009).

A series of resolution tests (Fig. S3) indicate that our data distribution allows to constrain along-strike variations of coupling on the subduction interface while along-dip variations cannot be resolved.

4.3 Results

4.3.1 3B models

Given the complex internal deformation (extension in the western part, dextral slip across the volcanic arc) within the CA block as defined in the 3B model, this model obviously cannot account for the observed GPS velocities on the CA block. We thus only consider the GPS vectors on the NA block for this first set of models.

We start from a simple parametrization of the MF and MAT (same coupling factor at all nodes for each fault) and progressively allow for potential along-strike variations in the coupling. The analysis of the residual velocities of this series of test models shows that, given our data distribution, a model with two sections along the MF (MF_e, MF_c for the east and central sections, respectively) as well as along MAT (MAT_{ch} and MAT_{gs} under Chiapas and Guatemala/El Salvador, respectively), is a good compromise to account for the observed GPS velocities (Fig. 7). Assuming a constant locking depth of 20 km all along the MF (see discussion in Section 3.2.1),

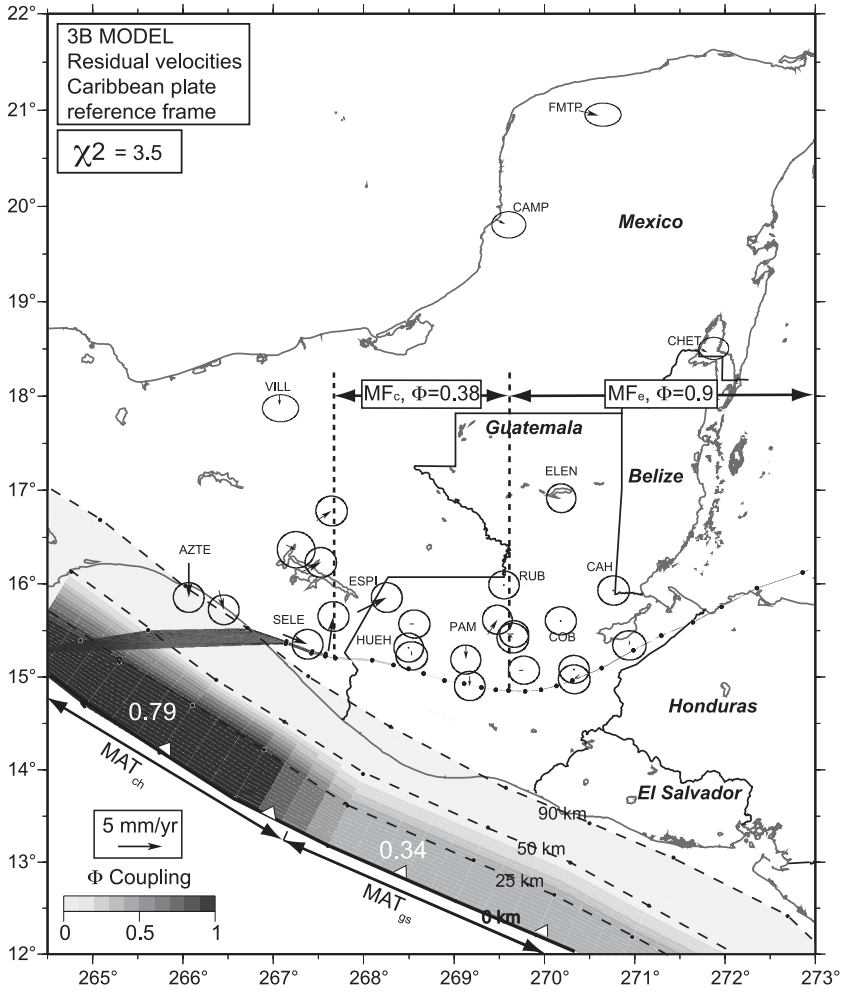

Figure 7. Inverted coupling coefficients along the MF_e, MF_c, MAT_{ch} and MAT_{gs}, and residual velocities for best-fitting 3B model.

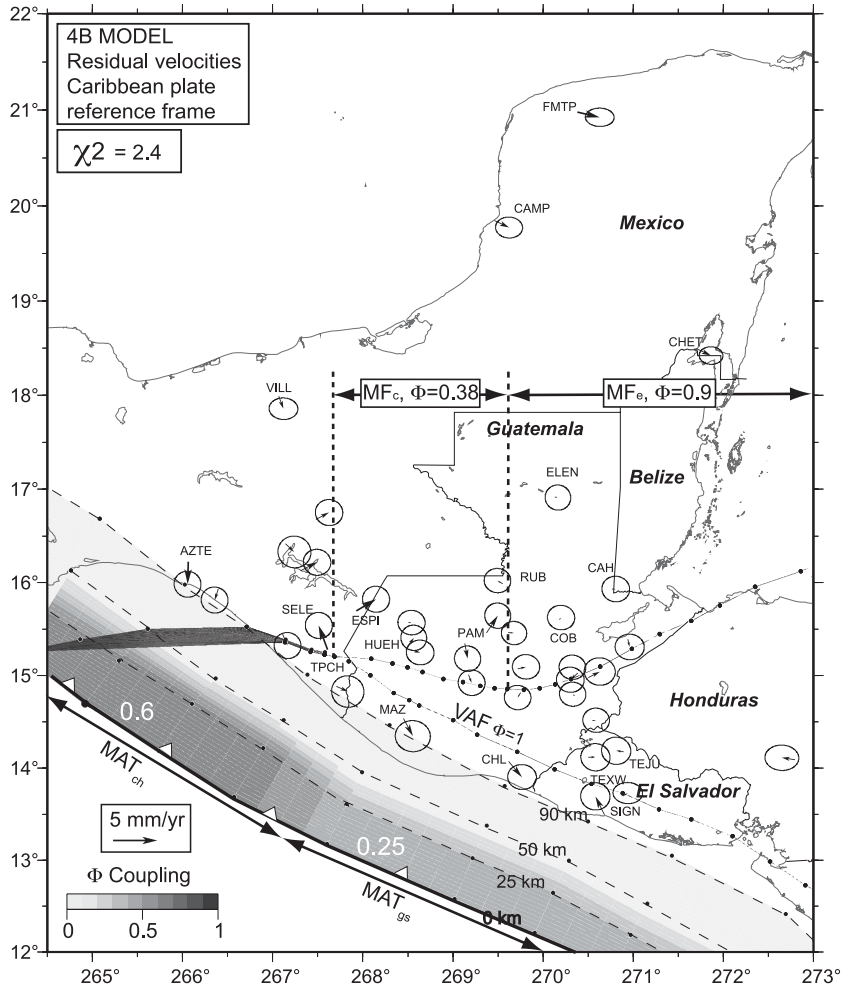

Figure 8. Same as Fig. 7 for best-fitting 4B model, with coupling along VAF fixed to 1.

the resulting 3B model shows a decreasing coupling on the fault from eastern ($\phi = 0.9$ along MF_e) to central ($\phi = 0.38$ along MF_c) Guatemala (Fig. 7). We interpret these coupling lateral variations as resulting from the westward velocity decrease on the MF. The coupling values correspond to average velocities of 18 and 8.5 mm yr^{-1} along the MF_e and MF_c, respectively. These velocities that represent average values on fault section are consistent with that deduced from the elastic half-space modelling on local profiles in Section 3.2.1. Fig. 7 also shows the resulting coupling along the subduction zone below Chiapas that is fairly high ($\phi = 0.79$ along MAT_{ch}) compared to the coupling below Guatemala and El Salvador ($\phi = 0.34$ along MAT_{gs}). This apparent contrast of coupling is better constrained and discussed from the 4B models later.

4.3.2 4B models

All GPS vectors are now inverted after fixing the coupling along the MF_e and MF_c to the values estimated in the previous section. Coupling along the VAF is considered uniform given our data distribution, although we would expect it to decrease westwards, as along the MF, due to the CA Plate internal extension.

Assuming first that the VAF is fully locked on the upper 15 km ($\phi_{VAF} = 1$, corresponding to a velocity of 15 mm yr^{-1}), the best-fitting model (Fig. 8) also shows lateral variations of coupling along the subduction zone as in model 3B, with a CO/NA high-coupling offshore Chiapas ($\phi = 0.61$ along MAT_{ch}), and a CO/AR low coupling south of the volcanic arc offshore Guatemala and El Salvador ($\phi = 0.25$ along MAT_{gs}). However, there is a trade-off in the inversion of the forearc velocity field between the contributions of the AR/CA rotation and the coupling along the VAF and MAT in Guatemala and El Salvador. To evaluate these relative contributions, we fix the CO/NA coupling ($\phi = 0.61$ along MAT_{ch}, Fig. 9) and run a series of inversion of the AR/CA angular velocity for different sets of coupling along the VAF and the MAT_{gs}. Note that in El Salvador, Correa-Mora *et al.* (2009) suggest that ϕ_{VAF} is larger than 0.85.

All best-fitting models indicate a CO/AR coupling ($\phi_{MAT_{gs}}$) around 0.25 ± 0.1, independently of the ϕ_{VAF} value (Fig. 9), confirming the contrast with the CO/NA coupling ($\phi_{MAT_{ch}}$). Pacheco *et al.* (1993) estimated a low-coupling value along the CO subduction interface (0.2), from the analysis of the cumulative seismic moment during the 20th century. However, this was an 'averaged' value from Chiapas to Costa Rica. A GPS-derived, low-coupling value offshore El Salvador was obtained more recently by Correa-Mora *et al.* (2009), consistent with our results.

5 CONCLUSION AND DISCUSSION

The new GPS measurements presented herein represent the first from the Chiapas region of Mexico, complement previous work from Guatemala and El Salvador, and enable the refinement of regional kinematic models previously proposed for the CO–NA–CA

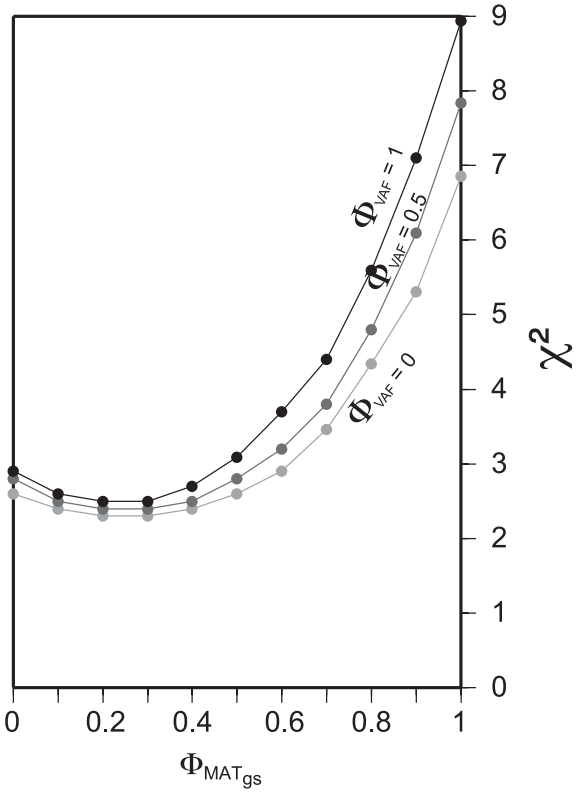

Figure 9. Reduced χ^2 as a function of $\phi_{\mathrm{MAT_{gs}}}$, for ϕ_{VAF} fixed to 0, 0.5 and 1. $\phi_{\mathrm{MAT_{ch}}}$ is fixed to 0.61. Only the Euler AR/CA rotation parameters are inverted.

plate triple junction (Plafker 1976; Lyon-Caen *et al.* 2006). The joint analysis of our results from the elastic half-space modelling (Section 3) and the DEFNODE block modelling (Section 4) of the GPS velocity field brings new constraints on the kinematics of the active structures as well as on the coupling along the subduction zone, as summarized in Fig. 10. Our results are in overall agreement with recent models based on GPS data in El Salvador, Honduras and Nicaragua and on geological and strain rate data (Alvarez-Gomez *et al.* 2008; Correa-Mora *et al.* 2009; Rodriguez *et al.* 2009).

5.1 Regional fault kinematics

The MF concentrates the present-day strain accumulation due to the NA/CA relative motion. The absence of resolvable strain accumulation across the active Polochic Fault cannot be explained in the modelling by post-seismic relaxation or rheological lateral variations. This suggests that slip on the PMF may vary with time as a result of mechanical interactions within this strike-slip fault system. Transient slip rate and activity switch between faults have already been observed from geodesy (east California shear zone, Peltzer *et al.* 2001), or from historical seismicity analysis and modelling (north and east Anatolian faults, Hubert-Ferrari *et al.* 2003).

The NA/CA motion decreases from 18–22 mm yr^{-1} in eastern Guatemala to 14–20 mm yr^{-1} in central Guatemala assuming a uniform locking depth of 14–28 km (best constrained by profile E, Fig. 4) and to ∼4 mm yr^{-1} in western Guatemala. West of the Mexican border, the MF likely connects with the Polochic Fault but does not accommodate any significant deformation. The east–west extension across the grabens in Guatemala at a rate of ∼9 mm yr^{-1} is mostly localized on the Guatemala city graben (∼5 mm yr^{-1}), whereas the remaining part is not clearly localized on specific grabens. A more complete discussion of the extension accommodation from western Guatemala to Honduras would require a joint

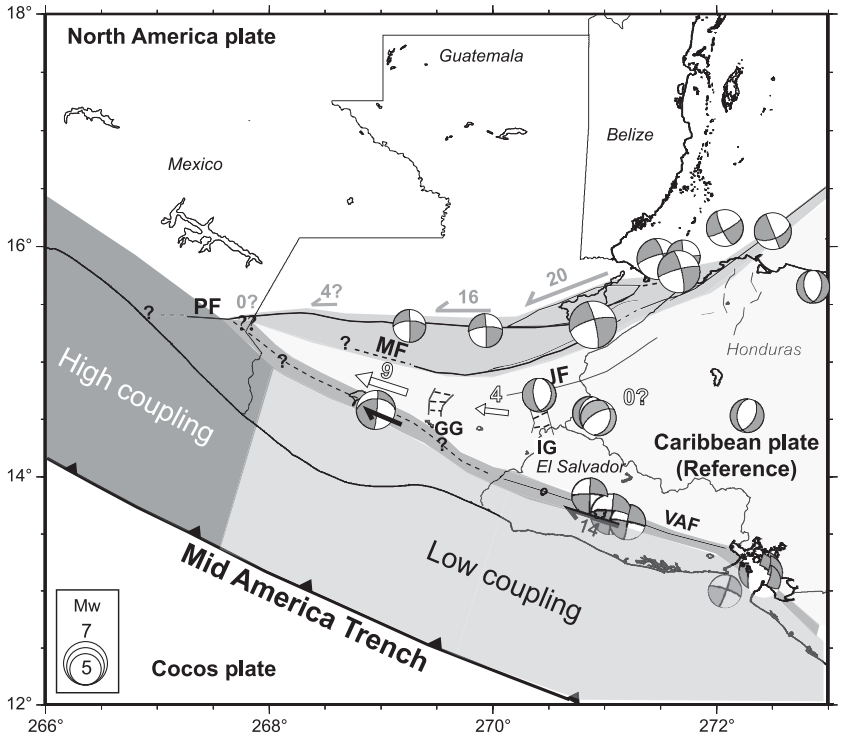

Figure 10. Proposed model of faults kinematics and coupling along the Cocos slab interface, revised from Lyon-Caen *et al.* (2006). Numbers are velocities relative to CA plate in mm yr^{-1}. Focal mechanisms are for crustal earthquakes (depth ≤30 km) since 1976, from CMT Harvard catalogue.

analysis of all regional GPS data in a common reference frame. Up to 15 mm yr^{-1} of dextral motion could be accommodated across the volcanic arc in El Salvador and southeastern Guatemala, consistent with estimations by Alvarado *et al.* (2011) in El Salvador and Nicaragua.

Kinematically, the extension in the western wedge of the CA Plate requires a westward decrease of both the PMF slip-rate and the VAF slip-rate (Fig. 10). This decrease can only be partly modelled herein given the limited spatial sampling of our velocity field.

5.2 Lateral coupling variation along the MAT

The coupling along the CO subduction zone varies along the MAT with a fairly high-coupling (∼0.6) offshore Chiapas and a low-coupling offshore Guatemala (∼0.25).

Lateral variations of coupling along subduction zones have been evidenced by cumulative seismic moment and geodetic studies in many areas (e.g. Pacheco *et al.* 1993). In recent years, the increasing space and time density of GPS data, in particular, have allowed to obtain maps of interseismic coupling along subduction interfaces, that are generally interpreted in terms of seismic hazard assessment, as in Sumatra (Prawirodirdjo *et al.* 1997; Chlieh *et al.* 2008), Kamchatka (Bürgmann *et al.* 2005), the Aleutian Islands (Cross & Freymueller 2007) or South America (e.g. Pritchard & Simons 2006; Ruegg *et al.* 2009; Perfettini *et al.* 2010). Segments with high coupling in the seismogenic zone are considered as the loci of large ($M > 8$) megathrust earthquakes, whereas segments with low coupling are associated with a seismic slip and moderate seismicity. Such along-strike variations of coupling are likely representative of heterogeneities in the mechanical properties at the interface. They are assumed to be rather stable in space and time through successive seismic cycles, although it may depend on their origin. A correlation between the degree of coupling and the age of the subducting lithosphere or the convergence rate has been suggested by Ruff & Kanamori (1980), in contradiction with more recent studies (Heuret & Lallemand 2005) and the occurrence of megathrust earthquakes in Sumatra (2004 Sumatra–Andaman) and Japan (2011 Tohoku-oki). High-coupling areas along subduction zones may be spatially correlated with forearc basins or thick sediments in the trench, and associated with negative free air-gravity anomalies (e.g. Ruff 1989; Song & Simons 2003; Wells *et al.* 2003; Bürgmann *et al.* 2005; Loveless *et al.* 2010). Low-coupling areas have also been correlated with the location of subducting ridges or seamounts (e.g. Cloos 1992).

The analysis of free-air gravity anomalies and marine seismic profiles offshore Mexico and Central America allows to derive a map of sediment thickness in this region (Divins 2003). Lateral variations of both Bouguer gravity anomalies and sediment thickness are observed offshore Chiapas and Guatemala (Fig. 11). The observed gradients, although rather low, would be consistent with, and may explain the coupling decrease at the subduction interface that we model (Fig. 8) from Chiapas to Guatemala and El Salvador (Song & Simons 2003). However, the historical seismicity, although poorly documented (White *et al.* 2004), does not reveal any clear lateral variations of the seismic behaviour along the subduction zone. Several M7.5–8.1 subduction earthquakes are reported, that seem to release less than 50 per cent of the accumulated slip (White *et al.* 2004). This would be consistent with the overall low-coupling values (0.25–0.6) that we model. The significance of such low values and of their lateral variations, in terms of seismic hazard for the study area, as well as their permanent or transient feature, thus remain open questions.

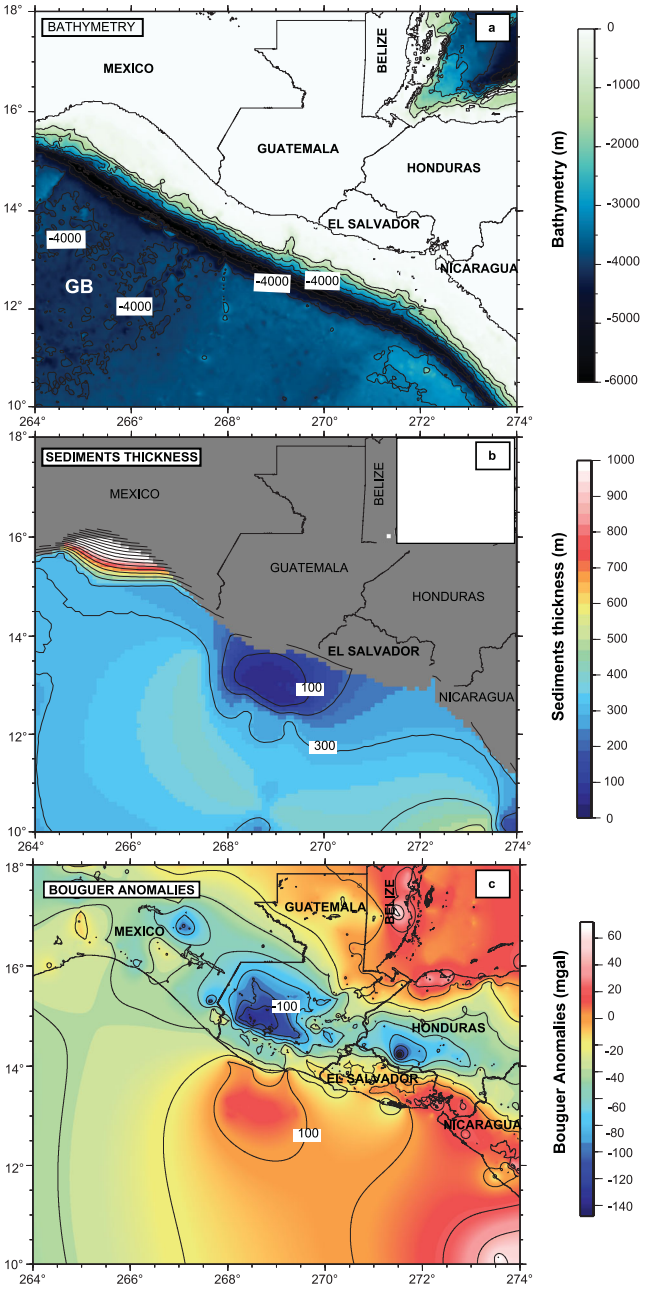

Figure 11. Maps of (a) bathymetry, (b) marine sediment thickness (Divins 2003; http://www.ngdc.noaa.gov/ngg/sedthick/sedthick.html) and (c) Bouguer gravity anomalies [calculated from raw data given by the Bureau Gravimétrique International (BGI)]. GB in (a) is for Guatemala Basin. See discussion in text.

ACKNOWLEDGMENTS

This work was partly funded by INSU-CNRS DyETI program. We thank the Guatemalan institutions INSIVUMEH, CONRED, IGN, CUNOR and CESEM from USAC, as well as the IGN in El Salvador, for their unvaluable logistic support. The french embassy in Guatemala provided help during field surveys. We thank Christophe Vigny for his help with GAMIT/GLOBK software and discussions concerning reference frames. We thank Christel Tiberi for help with the gravity data and Eric Calais for discussions concerning coupling on slab interface. We thank Charles DeMets and an anonymous reviewer for their constructive comments.

REFERENCES

Alvarado, D. *et al.*, 2011. Forearc motion and deformation between El Salvador and Nicaragua: GPS, seismic, structural, and paleomagnetic observations, *Lithosphere, **3***(1), 3–21, doi:10.1130/L108.1.

Alvarez-Gomez, J.A., Meijer, P.T., Martínez-Díaz, J.J. & Capote, R., 2008. Constraints from finite element modeling on the active tectonics of northern Central America and the Middle America Trench, *Tectonics,* **27,** doi:10.1029/2007TC002162.

Ambrasey, N.N. & Adams, R.D., 2001. *The Seismicity of Central America: A Descritive Catalogue 1898–1995,* Imperial College Press, London.

Bommer, J. *et al.*, 2002. The El Salvador earthquakes of January and February 2001: context, characteristics and implications for seismic risk, *Soil Dyn. Earthq. Eng.,* **22,** 389–418.

Bürgmann, R., Kogan, M.G., Steblov, G.M., Hilley, G., Levin, V. & Apel, E., 2005. Interseismic coupling and asperity distribution along the Kamchatka subduction zone, *J. geophys. Res.,* **110,** doi:10.1029/2005JB003648.

Burkart, F., 1978. Offset across the Polochic fault of Guatemala and Chiapas, Mexico, *Geology,* **6,** 251–270.

Burkart, F., 1983. Neogene North American-Caribbean plate boundary: offset along the Polochic fault, *Tectonophysics,* **99,** 328–332.

Burkart, F. & Self, S., 1985. Extension and rotation of crustal blocks in northern Central America and effect on the volcanic arc, *Geology,* **13,** 22–26.

Caceres, D., Monterroso, D. & Tavakoli, B., 2005. Crustal deformation in northern Central America, *Tectonophysics,* **404,** 119–131.

Canora, C., Martínez-Díaz, J.J., Villamor, P., Berryman, K., Álvarez-Gómez, J.A.A., Pullinger, C. & Capote, R., 2010. Geological and seismological analysis of the 13 February 2001 M_w 6.6 El Salvador earthquake: evidence for surface rupture and implications for seismic hazard, *Bull. seism. Soc. Am.,* **100**(6), 2873–2890.

Carfantan, J., 1986. Du domaine cordilliérain Nord-Américain au domaine Caraïbe : étude géologique du Mexique Méridional, *PhD thesis*, Université de Savoie, Chambéry.

Carr, M.J., 1976. Underthrusting and quaternary faulting in northern Central America, *Bull. geol. Soc. Am.,* **8**(5), 825–829.

Chéry, J., 2007. Geodetic strain across the San Andreas Fault reflects elastic plate thickness variations (rather than fault slip rate), *Earth planet. Sci. Lett.,* **269,** 352–365.

Chlieh, M., Avouac, J., Sieh, K., Natawidjaja, D. & Galetzka, J., 2008. Heterogeneous coupling of the Sumatra megathrust constrained by geodetic and paleogeodetic measurements, *J. geophys. Res.,* **113,** doi:10.1029/2007JB004981.

Cloos, M., 1992. Thrust type subduction-zone earthquakes and seamount asperities: a physical model for seismic rupture, *Geology,* **20,** 601–604.

Correa-Mora, F. *et al.*, 2009. Evidence for weak coupling of the Cocos plate subduction interface and strong coupling of the volcanic arc faults from modeling of GPS data: El Salvador and Nicaragua, *Geophys. J. Int.,* **179,** 1279–1291.

Corti, G., Carminati, E., Mazzarini, F. & Garcia, M.O., 2005. Active strike-slip faulting in El Salvador, Central America, *Geology,* **33,** 989–992.

Cross, R. & Freymueller, J., 2007. Plate coupling variation and block translation in the Andreanof segment of the Aleutian arc determined by subduction zone modeling using GPS data, *Geophys. Res. Lett.,* **34,** doi:10.1029/2006GL028970.

DeMets, C., 2001. A new estimate for present-day Cocos-Caribbean plate motion: implications for slip along the Central American volcanic arc, *Geophys. Res. Lett.,* **28**(21), 4043–4046.

DeMets, C., Gordon, R.G., Argus, D.F. & Stein, S., 1990. Current plate motions, *Geophys. J. Int.,* **101,** 425–478.

DeMets, C., Gordon, R.G., Argus, D.F. & Stein, S., 1994. Effect of the recent revisions to the geomagnetic reversal timescale on estimates of current plate motions, *Geophys. Res. Lett.,* **21,** 2191–2194.

DeMets, C., Jansma, P.E., Mattioli, G.S., Dixon, T.H., Farina, F., Bilham, R., Calais, E. & Mann, P., 2000. GPS geodetic constraints on Caribbean-North America plate motion, *Geophys. Res. Lett.,* **27**(3), 437–440.

DeMets, C., Mattioli, G., Jansma, P., Rogers, R., Tenorio, C. & Turner, H.L., 2007. Present motion and deformation of the Caribbean plate: constraints from new GPS geodetic measurements from Honduras and Nicaragua, in *Geologic and Tectonic Development of the Caribbean Plate in Northern Central America,* pp. 21–36, ed. Mann, P., Geol. Soc. Am. Spec. Paper 428, The Geological Society of America, Boulder, doi:10.1130/2007.2428(01).

Divins, D.L., 2003. Thickness of sedimentary cover in the Eastern Pacific Ocean, in *International Geological-Geophysical Atlas of the Pacific Ocean,* pp. 120, 126–127, 130, ed. Udintsev, G.B., Intergovernmental Oceanographic Commission, Moscow.

Farr, T.G. & Kobrick, M., 2000. Shuttle radar topography mission produces a wealth of data, *EOS, Trans. Am. geophys. Un.,* **81,** 583–585.

Feuillet, N., Manighetti, I., Tapponier, P. & Jacques, E., 2002. Arc parallel extension and localization of volcanic complexes in Guadeloupe, Lesser Antilles, *J. geophys. Res.,* **107**(B12), doi:10.1029/2001JB000308.

Franco, A. *et al.*, 2009. Seismicity and crustal structure of the Polochic-Motagua Faults System Area (Guatemala), *Seismol. Res. Lett.,* **80**(6), 977–984.

Guzmán-Speziale, M., 2001. Active seismic deformation in the grabens of northern Central America and its relationship to the relative motion of the North America-Caribbean plate boundary, *Tectonophysics,* **337,** 39–51.

Herring, T.A., 2002. GLOBK, Global Kalman filter VLBI and GPS analysis program, Version 10.0, Massachusetts Institute of Technology, Cambridge.

Heuret, A. & Lallemand, S., 2005. Plate motions, slab dynamics and back-arc deformation, *Phys. Earth planet. Inter.,* **149,** 31–51.

Hubert-Ferrari, A., King, G., Manighetti, I., Armijo, R., Meyer, B. & Taponnier, P., 2003. Long-term elasticity in the continental lithosphere; modelling the Aden Ridge propagation and the Anatolian extrusion process, *Geophys. J. Int.,* **153,** 111–132.

Jolivet, R., Cattin, R., Chamot-Rooke, N., Lasserre, C. & Peltzer, G., 2008. Thin-plate modeling of interseismic deformation and asymetry across the Altyn Tagh fault zone, *Geophys. Res. Lett.,* **35,** L02309, doi:10.1029/2007GL031511.

King, R.W. & Bock, Y., 2002. Documentation for the GAMIT GPS Analysis software, Mass. Inst. of Tech., Scripps Inst. Oceanogr., Release 10.0.

Kovach, R.L., 2004. *Early Earthquakes of the Americas,* Cambridge University Press, New York, 268pp.

LaFemina, P., Dixon, T. & Strauch, W., 2002. Bookshelf faulting in Nicaragua, *Geology,* **30,** 751–754.

LaFemina, P. *et al.*, 2009. Fore-arc motion and Cocos ridge collision in Central America, *Geochem. Geophys. Geosyst.,* **10,** Q05S14, doi:10.1029/2008GC002181.

Le Pichon, X., Kreemer, C. & Chamot-Rooke, N., 2005. Asymmetry in elastic properties and the evolution of large continental strike-slip faults, *J. geophys. Res.,* **110,** B03405, doi:10.1029/2004JB003343.

Loveless, J.P., Pritchard, M.E. & Kukowski, N., 2010. Testing mechanisms of subduction zone segmentation and seismogenesis with slip distributions from recent Andrean earthquakes, *Tectonophysics,* **495,** 15–33.

Lyon-Caen, H. *et al.*, 2006. Kinematics of the North America-Caribbean-Cocos plates in Central America from new GPS measurements across the Polochic-Motagua fault system, *Geophys. Res. Lett.,* **33,** doi:10.1029/2006GL027696.

Márquez-Azúa, B. & DeMets, C., 2009. Deformation of Mexico from continuous GPS from 1993 to 2008, *Geochem. Geophys. Geosyst.,* **10**(1), doi:10.1029/2008GC002278.

Martens, U. *et al.*, 2007. High-pressure Belts of Central Guatemala: The Motagua Suture and the Chuacs Complex. Field trip guide, *2007 Field Workshop of IGCP 546, Subduction Zones of the Caribbean Guatemala City,* 32pp.

Martínez-Díaz, J., Álvarez Gómez, J., Benito, B. & Hernández, D., 2004. Triggering and destructive earthquakes in El Salvador, *Geology,* **32,** 65–68.

McCaffrey, R., 2002. Crustal block rotations and plate coupling, in *Plate Boundary Zones,* Geodynamics Series Vol. 30, pp. 101–122, eds Stein, S. & Freymueller, J., American Geophysical Union Washington, DC.

Norabuena, E. *et al.*, 2004. Geodetic and seismic contraints on some seismogenic zone processes in Costa Rica, *J. geophys. Res.,* **109,** (B11403), doi:10.1029/2003JB002931.
Okada, Y., 1985. Surface deformation due to shear and tensile faults in a half-space, *Bull. seism. Soc. Am.,* **75,** 1135–1154.
Pacheco, J.F., Sykes, L.R. & Sholz, C.H., 1993. Nature of seismic coupling along simple plate boundaries of the subduction type, *J. geophys. Res.,* **98**(B8), 14 133–14 159.
Perfettini, H. *et al.*, 2010. Seismic and aseismic slip on the Central Peru megathrust, *Nature,* **465,** doi:10.1038/nature09062.
Plafker, G., 1976. Tectonic aspect of the Guatemala earthquake of 4 February 1976, *Science,* **193**(4259), 1201–1207.
Peltzer, G., Cramp, F., Hensley, S. & Rosen, P., 2001. Transient strain accumulation and fault interaction in the Eastern California shear zone, *Geology,* **29**(11), 975–978.
Prawirodirdjo, L. *et al.*, 1997. Geodetic observations of intersismic strain segmentation at the Sumatra subduction zone, *Geophys. Res. Lett.,* **24,** 2601–2604.
Pritchard, M.E. & Simons, M., 2006. An aseismic fault slip pulse in northern Chile and along-strike variations in seismogenic behavior. *J. geophys. Res.,* **111,** doi:10.1029/2006JB004258.
Rodriguez, M., DeMets, C., Rogers, R., Tenorio, C. & Hernandez, D., 2009. A GPS and modelling study of deformation in northern Central America. *Geophys. J. Int.,* **178**(3), 1733–1754.
Ruegg, J.C. *et al.*, 2009. Interseismic strain accumulation measured by GPS in the seismic gap between Constitución and Concepción in Chile, *Phys. Earth planet. Inter.,* **175,** 78–85.
Ruff, L., 1989. Do trench sediments affect great earthquake occurence in subduction zones?, *Pure appl. Geophys.,* **129,** 263–282.
Ruff, L. & Kanamori, H., 1980. Seismicity and subduction process, *Phys. Earth planet. Inter.,* **23,** 240–252.
Savage, J.C., 1983. A dislocation model of strain accumulation and release at a subduction zone, *J. geophys. Res.,* **88,** 4984–4996.
Savage, J.C. & Burford, R.O., 1973. Geodetic determination of relative plate motion in Central California, *J. geophys. Res.,* **78,** 832–845.
Schmalzle, G., Dixon, T., Malservisi, R. & Govers, R., 2006. Strain accumulation across the Carrizo segment of the San Andreas fault, California: impact of laterally varying crustal properties, *J. geophys. Res.,* **111,** B05403, doi:10.1029/2005JB003843.
Schwartz, D., Cluff, L. & Donnelly, T., 1979. Quaternary faulting along the Caribbean North American plate boundary in Central America, *Tectonophysics,* **52,** 431–445.
Smith, W.H.F. & Sandwell, D.T., 1997. Global seafloor topography from satellite altimetry and ship depth soundings, *Science,* **277,** 1957–1962.
Song, T.R.A. & Simons, M., 2003. Large trench-parallel gravity variations pedict seismogenic behaviour in subduction zones, *Science,* **301,** 630–633.
Suski, B., Brocard, G., Authemayou, C., Muralles, B.C., Teyssier, C. & Holliger, K, 2009. Localization and characterization of an active fault in an urbanized area in central Guatemala by means of geoelectrical imaging, *Tectonophysics,* **480,** 1–4.
Turner, H.L., LaFemina, P., Saballos, A., Mattioli, G., Jansma, P.E. & Dixon, T., 2007. Kinematics of the Nicaraguan forearc from GPS geodesy, *Geophys. Res.Lett.,* **34,** L02302, doi:10.1029/2006GL027586.
Vallée, M., Bouchon, M. & Schwarz, S.Y., 2003. The 13 January 2001 El Salvador earthquake: a multidata analysis, *J. geophys. Res.,* **108**(B4), 2203–2222.
Weber, J. *et al.*, 2001. GPS estimate of relative motion between the Caribbean and South American plates, and geologic implications for Trinidad and Venezuela, *Geology,* **29**(1), 75–78.
Wells, D. & Coppersmith, K., 1994. New empirical relationships among magnitude, rupture length, rupture width, rupture area, and surface displacement, *Bull. seism. Soc. Am.,* **84**(4), 974–1002.
Wells, R.E., Blakely, R.J., Sugiyama, Y., Scholl, D.W. & Dinterman, P.A., 2003. Basin-centered asperities in great subduction zone earthquakes: a link between slip subsidence, and subduction erosion, *J. geophys. Res.* **108**(B10), doi:10.1029/2002JB002072.
White, R., 1985. The Guatemala earthquake of 1816 on the Chixoy-Polochic fault, *Bull. seism. Soc. Am.,* **75,** 455–473.
White, R.A. & Harlow, D. H., 1993. Destructive upper-crustal earthquakes of Central America since 1900, *Bull. seism. Soc. Am.,* **83,** 1115–1142.
White, R.A., Logorría, J.P. & Cifuentes, I.L., 2004. Seismic history of the Middle America subduction zone along El Salvador, Guatemala and Chiapas, Mexico: 1526–2000, *Geol. Soc. Am., Spec. Paper,* **375,** 378–396, doi:10.1130/0-8137-2375-2.379.
Yu, T., Rundle, J.B. & Fernández, J., 1996. Surface deformation due to a strike slip fault in an elastic gravitational layer overlying a viscoelastic gravitational half space, *J. geophys. Res.,* **101**(B2), 3199–3214.

SUPPORTING INFORMATION

Additional Supporting Information may be found in the online version of this article:

Figure S1. (a) ITRF2000 velocity field for the Guatemala/El Salvador GPS subnetwork (black arrows), Chiapas subnetwork (grey arrows) and DeMets *et al.* (2007) solution (white arrows), before adjustment to a common reference frame (see processing strategy in text and Table S5). Inset shows common IGS permanent sites used in GLOBK (squares) and for reference frame adjustment (circles) for both Guatemala/El Salvador and Chiapas solutions. (b) ITRF2000 velocity field after adjustment (see Table 1).
Figure S2. Cumulative post-seismic displacements, estimated along a profile perpendicular to the Motagua Fault, for each GPS campaign in 1999, 2003 and 2006, corresponding to 23, 27 and 30 yr after the 1976 Guatemala earthquake, respectively, and for viscosity of 10^{18}, 10^{19}, 10^{20} and 10^{21} Pa s.
Figure S3. Resolution tests for 3B models. (a) Forward model imposing along-strike and along-dip coupling variations along the subduction zone. (b) Coupling inverted from (a) and residual velocities. The synthetic GPS vectors obtained in (a) are associated with uncertainties from Table 1, and inverted for coupling along the MAT (all other parameters are fixed). Along-dip variations cannot be retrieved. (c) Same as (a) with along-strike variations of coupling only. (d) Same as (b). Lateral variations are well retrieved by inversion.
Table S1. Occupation history of campaign GPS sites.
Table S2. Cumulative coseismic displacement modelled at each station, for all events that occurred between 1999–2006 or 2003–2006. No estimate was done for sites ELEN, GUAT and SSIA (we use velocities computed by DeMets *et al.* 2007).
Table S3. Coseismic displacement (mm) modelled at each station, for each event that occurred between 1999–2006 or 2003–2006. Each earthquake is named after its reference in the CMT Harvard catalogue.
Table S4. Angular velocities used in this study. Ref 1: DeMets *et al.* (2007), Ref 2: DeMets et *al.* (1990) and (1994).
Table S5. Rotation parameters used to adjust the Guatemala/El Salvador, Chiapas, and DeMets *et al.* (2007) solutions in the same reference frame.

Please note: Wiley-Blackwell are not responsible for the content or functionality of any supporting materials supplied by the authors. Any queries (other than missing material) should be directed to the corresponding author for the article.